

Effects of Odd–Even Side Chain Length of Alkyl-Substituted Diphenylbithiophenes on First Monolayer Thin Film Packing Structure

Hylke B. Akkerman,^{†,‡} Stefan C. B. Mannsfeld,[‡] Ananth P. Kaushik,[§] Eric Verploegen,^{†,‡} Luc Burnier,[§] Arjan P. Zoombelt,[†] Jonathan D. Saathoff,[§] Sanghyun Hong,^{†,⊥} Sule Atahan-Evrenk,^{||} Xueliang Liu,^{||} Alán Aspuru-Guzik,^{||} Michael F. Toney,[‡] Paulette Clancy,[§] and Zhenan Bao^{*,†}

[†]Department of Chemical Engineering, Stanford University, Stauffer III, 381 North–South Mall, Stanford, California 94305-5025, United States

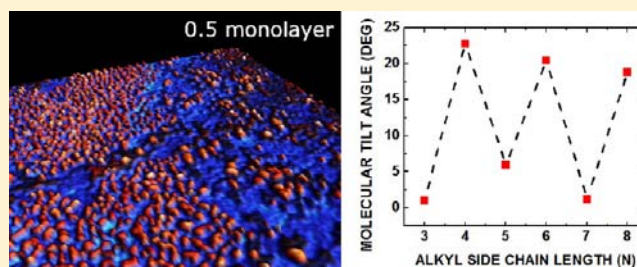
[‡]Stanford Synchrotron Radiation Laboratory, 2575 Sand Hill Road, Menlo Park, California 94025, United States

[§]School of Chemical and Biomolecular Engineering, Cornell University, 120 Olin Hall, Ithaca, New York 14853-5201, United States

^{||}Department of Chemistry and Chemical Biology, Harvard University, 12 Oxford Street, Cambridge, Massachusetts 02138, United States

S Supporting Information

ABSTRACT: Because of their preferential two-dimensional layer-by-layer growth in thin films, 5,5'-bis(4-alkylphenyl)-2,2'-bithiophenes (P2TPs) are model compounds for studying the effects of systematic chemical structure variations on thin-film structure and morphology, which in turn, impact the charge transport in organic field-effect transistors. For the first time, we observed, by grazing incidence X-ray diffraction (GIXD), a strong change in molecular tilt angle in a monolayer of P2TP, depending on whether the alkyl chain on the P2TP molecules was of odd or even length. The monolayers were deposited on densely packed ultrasmooth self-assembled alkane silane modified SiO₂ surfaces. Our work shows that a subtle change in molecular structure can have a significant impact on the molecular packing structure in thin film, which in turn, will have a strong impact on charge transport of organic semiconductors. This was verified by quantum-chemical calculations that predict a corresponding odd–even effect in the strength of the intermolecular electronic coupling.



INTRODUCTION

A range of low-cost and large-area applications are emerging from the field of organic electronics, such as solid-state lighting,^{1,2} solar cells,^{3,4} and displays.^{5,6} Different performance parameters such as luminescence efficiency in organic light-emitting diodes (OLEDs), power conversion efficiency in organic photovoltaic cells (OPV), or field-effect mobility in organic field-effect transistors (OFETs) are strongly determined by the morphology of the thin films and by the packing and orientation between individual molecules.^{7–11} Specifically, molecular packing strongly impacts the electronic coupling between molecules and the resulting charge carrier mobility.^{12,13} As a result, developing and understanding methods to control molecular packing of organic semiconductors by molecular design as well as processing control have been actively pursued by many research groups.^{14–22} In particular, we have been interested in molecular design rules for controlling thin film packing structures. We have been able to determine the precise molecular packing structures for thin films of pentacene, TIPSE-pentacene, and a series of fluorine–bithiophene oligomers from grazing incidence X-ray diffraction

(GIXD) data combined with numerical fitting.^{22–24} This development is important for structure–property relationship studies because it allows us to understand organic semiconductor packing on substrates that are directly used for device fabrication.

One of the common strategies to promote a more favorable two-dimensional growth is to substitute the two ends of a small molecule organic semiconductor with linear alkyl chains, which results in large and more connected grains. Indeed, using this approach, higher thin film transistor mobilities have been reported for sexithiophene (a-6T),²⁵ fluorene–bithiophene–fluorene (FTTF),^{26,27} acene derivatives,²⁸ [1]benzothieno[3,2-*b*]benzothiophene (BTBT),²⁹ and naphthalenetetracarboxylic diimide (NTCDI),^{30,31} just to name a few. So far, mostly even-numbered linear alkyl chains have been used. We hypothesized that organic semiconductor molecules with odd- and even-numbered alkyl chain substituents may result in different molecular packing and tilt angles on a smooth substrate surface,

Received: January 2, 2013

Published: July 4, 2013

an “odd-even” effect. Indeed, odd–even effects have been observed for self-assembled alkanethiol self-assembled monolayers (SAM) on gold surfaces resulting in different water contact angles.³² These odd- and even-numbered SAMs were also found to give rise to different liquid crystal molecular orientations for films deposited above them.³³ Therefore, in this work, we investigate, both theoretically and experimentally, the odd–even effects of organic semiconductor side chain length, as well as the dielectric surface modification with alkane silanes, on the molecular packing and the charge transport. Such studies are important since for charge transport, minor changes in molecular packing structures can have a significant impact on charge transport. Hence, this understanding may provide new insights for molecular design of organic semiconductors.

Herein, we have employed a series of 5,5′-bis(4-alkylphenyl)-2,2′-bithiophene (P2TP) molecules, with varying side chain length (3–8 methyl units; see Figure S1 in the Supporting Information for chemical structures), as the organic semiconductors. P2TPs exhibit a two-dimensional layer-by-layer growth when thermally evaporated and are known to form thin films with a preferential long axes of the molecule standing upright.^{34,35} Charge carrier mobility greater than 0.1 cm²/(V s) has been reported.^{34–36}

In organic thin film-based field-effect transistors (FETs), the charge transport occurs in the first few nanometers of the semiconductor at the dielectric-organic interface.^{34,37} Therefore, the choice of dielectric material strongly influences the charge transport in an FET because it determines the morphology of the semiconductor and the possible presence of energetic traps at the interface.^{8,38,39} In particular, the presence of hydroxyl groups on the commonly used Si/SiO₂ substrates strongly influences the mobility of charges in the transistor channel due to charge trapping^{40–42} and limits the operational stability of organic FETs due to a reversible proton migration from the semiconductor to the dielectric.^{43,44} To encapsulate the hydroxyl traps, the Si/SiO₂ substrates are frequently treated with hydrophobic monolayers, such as OTS.^{41,45} Previously, we have shown that a preferable, more two-dimensional, layer growth of thermally evaporated organic semiconductors is achieved when the density of octadecyltrimethoxysilane (OTMS) on the Si/SiO₂ substrate is increased.⁴⁶ Moreover, spin-coated OTMS can form crystalline self-assembled monolayers (SAMs) on amorphous SiO₂, leading to a highly enhanced two-dimensional growth of the semiconductor.⁴⁷ The crystalline OTMS was shown to result in a much lower surface roughness compared to vapor-deposited OTMS.⁴⁷ The improved organic semiconductor thin film morphology on crystalline OTMS results in transistors with an increased field-effect mobility by approximately an order of magnitude.^{46,47} Since the dielectric surface is very important for controlling the growth of the organic semiconductor, this study will involve the investigation of varying the organic semiconductor side chain odd–even effects in conjunction with Si/SiO₂ dielectric surfaces treated with crystalline heptadecyltrimethoxysilane (HDTs, C17) and octadecyltrimethoxysilane (ODTs, C18) SAMs.

RESULTS AND DISCUSSION

Fabrication of crystalline SAMs and devices was carried out according to previously published procedures.^{46,47} On highly n-doped silicon wafers with 300 nm thermally grown oxide, a crystalline monolayer of HDTs or ODTs was formed from solution. The crystalline monolayers of HDTs and ODTs

exhibit very similar surface properties, with a water contact angle of around 108° and a mean surface roughness (RMS) of ~0.3–0.4 nm (see the Supporting Information, Figures S2 and S3).

Grazing incidence X-ray diffraction characterizations of the HDTs and ODTs were performed to confirm the crystalline nature of the SAMs. Bragg rods were found at discrete in-plane momentum transfer values (q_{xy}) from which the dimensions of the HDTs and ODTs monolayer unit cells were determined. The diffraction images of ODTs and HDTs contain a Bragg rod at q_{xy} of around 1.50 and 1.51 Å⁻¹, respectively. This Bragg rod is due to the degenerate {01}, {10}, and {-11} diffraction peaks of the hexagonal lattice formed by the crystalline ODTs and HDTs monolayers (see Figure 2A). The corresponding ODTs and HDTs lattice constants of 4.84 and 4.81 Å are consistent with previous findings.⁴⁶ That the Bragg rod intensity peaks very close to $Q_z = 0$ implies that the molecules are standing nearly upright (untilted).

To study the growth of the first layer of P2TP molecules, we evaporated submonolayer P2TP films on HDTs and ODTs, respectively. The conditions for vacuum deposition are listed in Table 1. To achieve a highly two-dimensional layered growth,

Table 1. Thermal Evaporation Conditions for Half a Monolayer Coverage of C_N-P2TP-C_N

molecule	substrate temp (°C)	evap thickness (nm)
C3-P2TP-C3	46	1.05
C4-P2TP-C4	53	1.2
C5-P2TP-C5	60	1.3
C6-P2TP-C6	68	1.45
C7-P2TP-C7	76	1.55
C8-P2TP-C8	84	1.7

the substrate temperature, T_{sub} , was chosen to be 60 °C for 5,5′-bis(4-pentylphenyl)-2,2′-bithiophene (C₅-P2TP-C₅). Hereafter, molecules with a side chain length of N methyl units will be abbreviated as C _{N} -P2TP-C _{N} . For the heavier, longer molecules, higher substrate temperatures were chosen (Table 1) to offset the higher molecular weight and thus facilitate thermally activated molecular surface diffusion that is less dependent on the molecular weight.

Figure 1 shows atomic force microscopy (AFM) images of the corresponding films, with images A–F showing the layers evaporated on HDTs and images G–L evaporated on ODTs, respectively.

We found a surprising difference in the initial growth mode between the P2TP layers on HDTs and ODTs. With the exception of C₈-P2TP-C₈, all P2TP molecules on ODTs showed areas of initially flat-lying molecules (indicated by the black regions in Figures 1G–K) in the first layer on ODTs, whereas no indication for flat-lying molecules was found in the P2TP films on HDTs. Since every image of P2TPs on ODTs showed clusters of grains comprised solely of standing-up molecules, it is possible that when the molecule–molecule interaction is stronger than the molecule–surface interaction the flat-lying molecules diffuse over the surface and flip upright near the edge of an island of upright oriented molecules. This hypothesis is compatible with the complete absence of any scattering signal in the GIXD images that could be attributed to a second, crystalline phase of lying molecules, though this could also be due to lack of any crystalline ordering in the lying phase.

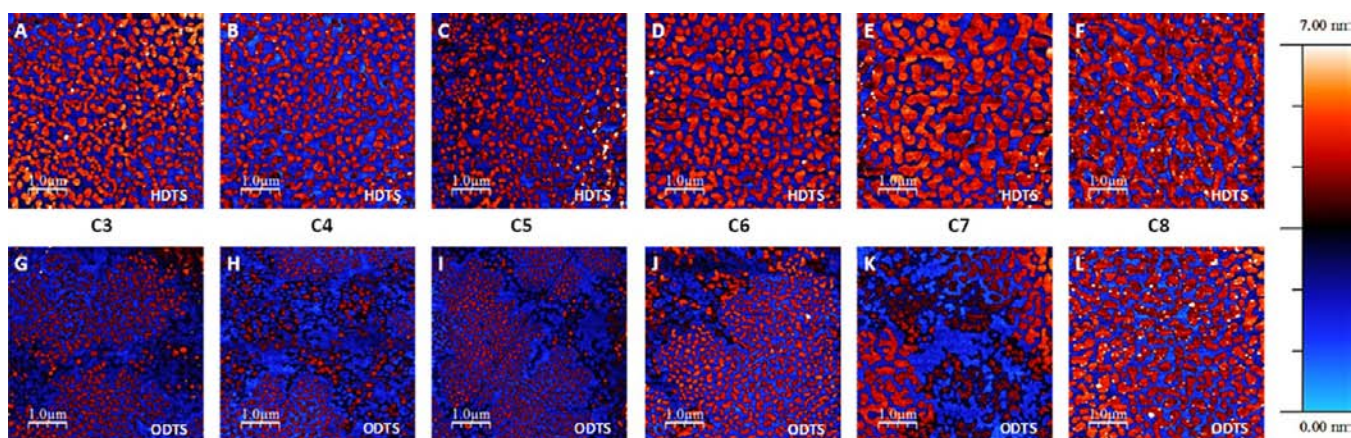


Figure 1. Images by atomic force microscopy (AFM) on a half monolayer coverage of C_N -P2TP- C_N , with N ranging from 3 to 8 methyl units in length. A-F depict the layers evaporated on HDTs treated substrates and G-L the layers of ODTS. The noncovered substrate is shown as blue. An increase in grain size (red) with increasing side chain length is observed. A second flat lying phase (black) on ODTS substrates is present but does not form on HDTs treated substrates.

It is also consistent with Molecular Dynamics simulations of similar molecules.⁴⁸

With increasing side chain length, from three methyl units up to eight (indicated by C3–C8), we observed an increase in apparent domain size as seen in AFM. As shown in Figure S4 (Supporting Information), we observed an increasing grain size of C_8 -P2TP- C_8 with substrate temperature from room temperature to 115 °C, indicating substrate temperature as a large contributor to the increase in grain size. However, we also observed an increased grain size with molecular chain length for 40 nm films evaporated at 60 °C (see Figure S5, Supporting Information), clearly indicating an effect of side chain length on grain size. The same trend was previously observed for oligoacenes^{49,50} and oligothiophenes,⁵¹ where higher aspect molecules tend to form more two-dimensional films with large islands. Larger islands are the result of a lower nucleation density, which in the case of longer molecules, originates from molecule–molecule interactions that are increased relative to the molecule–substrate interactions. The molecule–substrate interactions are similar for all P2TP derivatives and dominated by the interactions between the terminal methyl group and the substrate surface.

Grazing incidence X-ray diffraction characterization of the C_N -P2TP- C_N films was performed to determine the unit cells and corresponding molecular packing inside these unit cells on HDTs and ODTS substrates. These cell dimensions were obtained from the measured in-plane diffraction peak positions by using a least-squares error minimization algorithm. Besides the peaks that were attributed to the C_N -P2TP- C_N submonolayers, the diffraction images of all investigated films showed an additional broad peak at around 1.50 \AA^{-1} that corresponds to a hexagonal lattice of the densely packed HDTs and ODTS films, which confirms that crystalline HDTs and ODTS SAMs were indeed present in all samples and that the crystalline structure of the SAMs were not altered by the growth of the P2TP derivatives. The motif by which the molecules pack inside the C_N -P2TP- C_N unit cells was extracted by crystallographic refinement of the diffraction intensity data obtained from these Bragg rods. This was achieved by fitting calculated diffraction intensities to the measured intensity data, see Figure 2B. Several corrections to the theoretical scattering intensity need to be taken into account, as explained in the Supporting Information.

Even without the crystallographic refinement, the diffraction data in Figure 2A show the odd–even effect. For C_3 -P2TP- C_3 , the Bragg rod intensity peaks near $Q_z = 0$, and from this, we can immediately conclude that the molecules are nearly standing upright.⁵² For C_4 -P2TP- C_4 , the Bragg rod intensity for the (02) peaks near $Q_z = 0.6 \text{ \AA}^{-1}$, which would give a tilt angle of about 22° ($\text{atan}(0.6/1.5)$), assuming the molecule tilts along the b -axis, which is justified since the (11) Bragg rod has a maximum intensity at $Q_z = 0.3 \text{ \AA}^{-1}$ ($1/2$ of 0.6 \AA^{-1}). This approximate calculation ignores complications due to the molecular structure (e.g., it assumes a cylindrical molecule as for many Langmuir monolayer films), but it provides a semiquantitative picture that supports the more detailed calculations below.

Minimization of the crystallographic residual was performed by in-house software POWERGRID which implements the Monte Carlo Simulated Annealing method.²² For this refinement, integrated intensities $I(q_z)$ were measured along the Bragg rods, and the molecular alignment varied until the best agreement between measured and calculated intensities is achieved. Only the clearly measurable rods were included in the fit (typically {11}, {02}, {12}, but in some cases only {11} and {02}). In addition, owing to the significance of the absence of the {01} and {10} for the symmetry in the molecular-packing motif, the {01} and {10} rods were included in the calculation and set to zero. For the computation to be feasible, the C_N -P2TP- C_N molecules were treated as rigid objects. This assumption is justified only in case of the shorter alkyl chain derivatives since alkyl chains beyond a certain length (we estimate >4 methyl groups) possess inherent flexibility that is not properly captured by the rigid molecule approximation. Specifically, while good structural refinements could be obtained for C_N -P2TP- C_N with $N = 3, 4, 5$, the fits became increasingly worse for the longer derivatives ($N = 6, 7, 8$). However, for two reasons, the crystallographic refinement can still be performed, even for the longer chain derivatives: (i) a significant portion of the peak intensity is determined by the heavy sulfur atoms on the essentially rigid P2TP backbone (geometry-stabilized by the π - π^* interactions between the aromatic carbon atoms) that scatter far stronger than the carbon atoms and (ii) the alkyl chains, especially the longer ones, do not necessarily contribute significantly to the peak intensity (due to disorder) but rather create a diffuse scattering

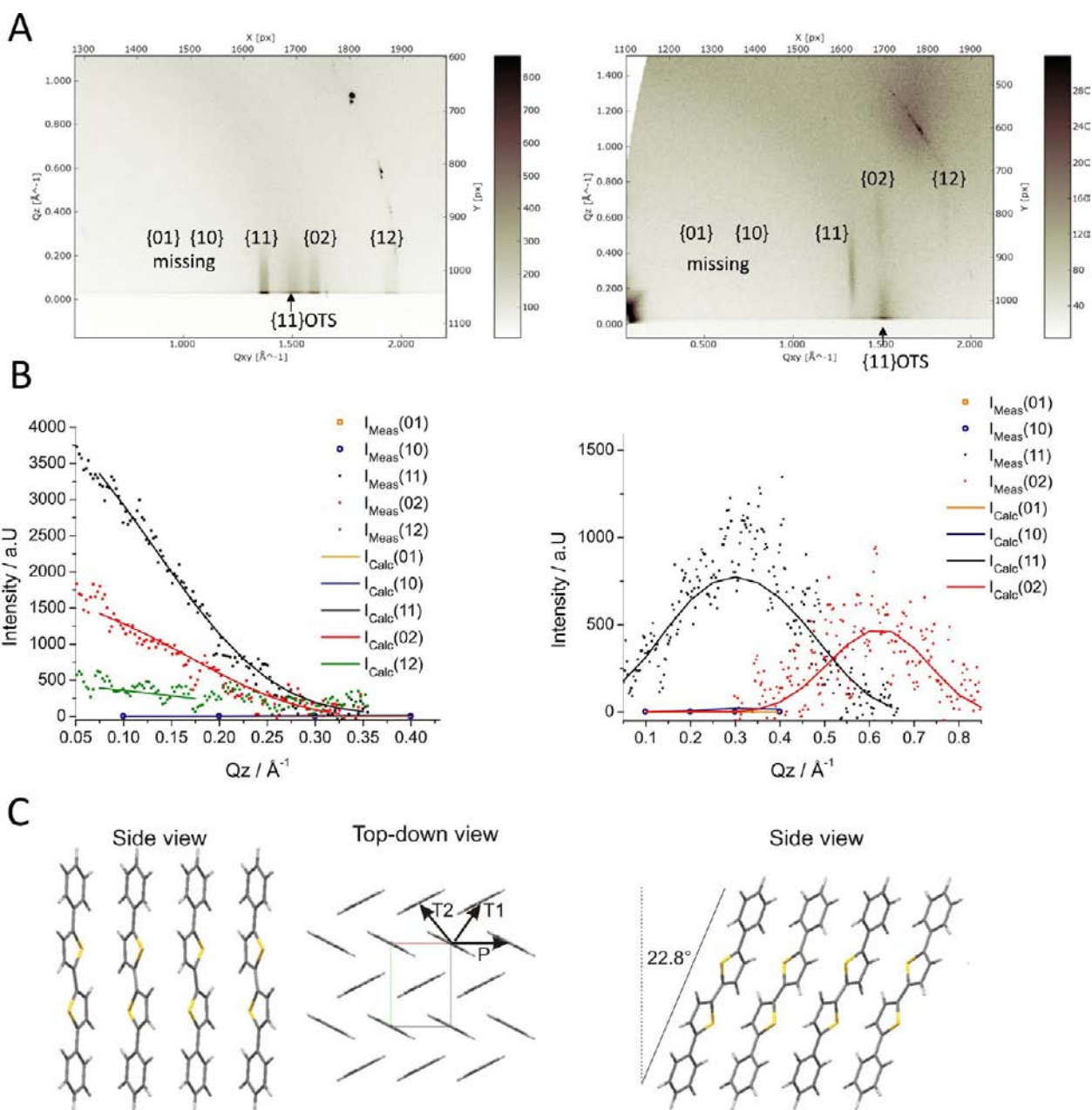


Figure 2. (A) GIXD spectra of half a monolayer of C_3 -P2TP- C_3 and C_4 -P2TP- C_4 on ODTs. Significant differences in dependence of the intensity on Q_z are visible for the $\{11\}$, $\{02\}$, and $\{12\}$ Bragg rods, showing the structural odd-even effect. (B) Best fit of the theoretically calculated diffraction intensities to the experimentally obtained data of half a monolayer of C_3 -P2TP- C_3 and C_4 -P2TP- C_4 on ODTs (left and right, respectively). (C) Best-fit packing from the calculated GIXD spectra of C_3 -P2TP- C_3 and C_4 -P2TP- C_4 on ODTs. In all cases, the P2TP cores adopt a herringbone packing in the unit cell (see Top-down view of C_3 -P2TP- C_3). However, while in C_3 -P2TP- C_3 films the P2TP core is perpendicular to the substrate, the P2TP core in C_4 -P2TP- C_4 films is tilted about 23° , mainly in the direction of the b unit cell axis.

background. Therefore, we assumed the intensity along the Bragg rods to be mostly determined by the alignment of the P2TP core alone. The quality of the fit between theoretical and experimental intensity profiles when the fitting was performed for the P2TP core only (see Figure 2B) supports this conclusion. The molecular geometry of the P2TP core was calculated using the Parametric Model no. 3 (PM3) semi-empirical method. Besides an overall scaling factor, 10 degrees of freedom were considered in the optimization: three Euler angles for each P2TP molecule, three coordinates describing the position of the second molecule relative to the first one, and the molecular mean square displacement $\langle U^2 \rangle$. Thus, no

artificial constraint was placed on the molecular positions in the unit cell.

The best-fit theoretical $I_{hk}(q_z)$ functions and the corresponding experimental $I_{hk}(q_z)$ values are displayed in Figure 2B; the corresponding arrangement of the two C_N -P2TP- C_N molecules after 2.5 million Monte Carlo steps is shown in Figure 2C. The optimization was repeated numerous times, leading to identical best-fit configurations in all runs. For all chain lengths where the Bragg profiles were refined ($N = 3-8$), the unit cell contains two P2TP molecules that are aligned in the well-known herringbone pattern (see center of Figure 3C) whose two glide-symmetry planes explain the absences of

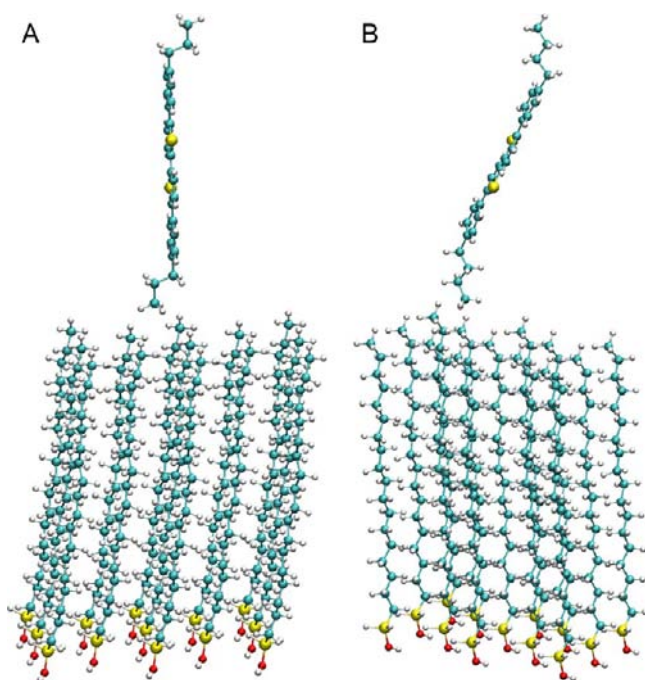


Figure 3. Lowest energy position of P2TP on top of ODTS: (A) C_3 -P2TP- C_3 molecules with a tilt angle of 5° ; (B) C_4 -P2TP- C_4 under a tilt angle of 19° .

diffraction intensity in the $\{01\}$ and $\{10\}$ rods. This arrangement is common in most linear aromatic molecules, for example, pentacene.²³ Note the weak intensity of the $\{20\}$ Bragg rod in the GIXD images in Figure 2. This results from the rather uniform electron density along the a -direction as can be seen in the top-down view in Figure 2.

A clear odd–even effect is obtained for both the long unit cell axis b and the tilt angle of the P2TP core with respect to the substrate surface normal (see Table 2). For the three odd-

Table 2. Unit Cell Geometries and P2TP Core off-Normal Tilt Angle on ODTS by GIXD (Experimental Uncertainty <0.01 Å, for Both a and b)

side chain length N	a (Å)	b (Å)	γ (deg)	tilt angle (deg)
3	5.66	7.85	89.9	1.01
4	5.70	8.46	90.0	22.79
5	5.70	7.86	90.0	5.95
6	5.71	8.42	90.0	20.41
7	5.74	7.81	90.2	1.20
8	5.72	8.21	90.6	18.8

length derivatives, in which $N = 3, 5,$ or $7,$ the b axis is shorter, at around 7.8 Å, and the tilt angle is small, i.e., the P2TP core is nearly vertical relative to the substrate. In contrast, the b axis in the case of the even length molecules, in which $N = 4, 6,$ or 8 is substantially longer (8.2 – 8.4 Å), and the molecules are significantly more tilted, with tilt angles around 20° , as shown for C_4 -P2TP- C_4 in the right part of Figure 3C. The concurrent increase in b axis length and tilt angles for the even-chain length derivatives is consistent with the finding that the tilt of the P2TP cores is almost exclusively in the direction of the b axis. Because of the tilt, the projection of the molecules in the substrate surface plane is larger and, consequently, the unit cell is expanded in the tilt direction, i.e., the b axis. The GIXD intensity profiles, and consequently, the P2TP molecular

packing structures of C_N -P2TP- C_N submonolayers on HDTS are nearly identical to those on ODTS, suggesting identical growth of C_N -P2TP- C_N on the two substrates. This was verified in fits for C_3 -P2TP- C_3 and C_4 -P2TP- C_4 on HDTS that yielded tilt angles and packing motifs that were practically identical to those on ODTS.

To provide insight into the mechanism leading to the odd–even effect, we performed simulations of the system using Molecular Dynamics (MD) computations. Experimental length scales are inaccessible using MD simulations; a tractable-sized system in the simulation is composed of a herringbone lattice consisting of 60 – 80 P2TP molecules. Periodic boundaries were employed in the lateral x - and y -directions, which simulate infinite 2D lattice structures efficiently and remove edge effects. In this system, alkylated P2TP molecules with an optimal lattice configuration (described in the Supporting Information) were placed on top of a thermalized ODTS surface at a distance between the long-axis of the P2TP and the ODTS surface of approximately 3 Å, corresponding to the minimum of the van der Waals interactions. At the start of the simulation, all the atoms were fixed, corresponding to a temperature of 0 K, before the ensemble was thermalized at 300 K for about 100 ps, which is enough for the SAM surface to equilibrate. The density of the simulated ODTS monolayer was chosen to be 5 molecules/nm² (the same as the experimental density), and resulted in a tilt angle of $6 \pm 2^\circ$ for the ODTS molecules. This value matches the experimentally observed tilt angle. Based on the nearly identical GIXD diffraction signals from both ODTS and HDTS films, the same molecular density was also chosen for HDTS. The deposition of a P2TP molecule on a SAM can, in principle, involve different possible outcomes, such as the insertion of the molecule in the SAM, adsorption on the surface, or scattering of the molecule.⁵³ However, due to the high density of the ODTS monolayer, insertion is unlikely.^{53,54} Scattering does not affect growth habit, and hence only the surface adsorption effect is important here. Additional details of the simulations are provided in the Supporting Information.

Table 3 shows the lattice parameters and tilt angles obtained from simulations. The simulations show a clear difference in tilt

Table 3. Unit Cell Geometries and P2TP off-Normal Tilt Angle by Simulations on SAMs

side chain length N	a (Å)	b (Å)	tilt angle (deg)
3	5.77 ± 0.3	7.90 ± 0.3	3.5 ± 1.5
4	6.12 ± 0.3	8.07 ± 0.3	19 ± 1.5
5	5.85 ± 0.3	7.60 ± 0.3	4.2 ± 1.5
6	5.61 ± 0.3	9.37 ± 0.3	19 ± 1.5
7	5.85 ± 0.3	7.65 ± 0.3	4.5 ± 2
8	5.63 ± 0.3	9.64 ± 0.3	22 ± 2

angle between odd- and even- side chain lengths, that closely mirrors experimental findings by GIXD. Predictions of a and b determined by simulation may not reproduce each individual experimental value, but the mean values of a and b are well within experimental error. More importantly, a distinct trend for b to oscillate between smaller and larger values for odd and even N values is seen in both experiments and simulation. This odd–even oscillation occurs because there is a significant energetic advantage for each set of C_N -P2TP- C_N molecules to orient themselves to a characteristic tilt angle. For example, for $N = 4$, i.e., C_4 -P2TP- C_4 , the lowest energy occurs when the molecule is tilted by 19° (a 2 kcal/mol advantage relative to a

tilt-free alignment, and a difference in the central energy maximum of 11 kcal/molecule). Furthermore, the position of lowest energy for both odd- and even-numbered side chain molecules lies in-between the terminal methyl groups of ODTS (not on top of ODTS).

A question that remains is whether this odd–even effect is due to the C_N –P2TP– C_N –SAM interactions alone or due to preferences for distinctly different crystal structures (say, herringbone and honeycomb) between molecules with odd- and even-numbered side chains. To answer this question, 2D crystals of the C_N –P2TP– C_N molecules *without* SAMs present were simulated. The simulation protocol described in the Supporting Information includes a section in which changes to the lattice parameters adopted by the P2TP molecules were permitted. Despite the additional freedom of the P2TP molecules to reorient if energetically advantageous, the crystals continued to exhibit herringbone packing for both odd- and even- length chains. Table 4 shows the predicted lattice

Table 4. Unit Cell Geometries and P2TP off-Normal Tilt Angle by Simulations without SAMS

side chain length N	a (Å)	b (Å)	tilt angle (deg)
3	5.68 ± 0.3	8.67 ± 0.4	16 ± 2.9
4	5.63 ± 0.3	10.19 ± 0.7	26 ± 4.3
5	5.66 ± 0.3	8.59 ± 0.4	8 ± 2.3
6	5.15 ± 0.3	6.55 ± 0.5	10 ± 2.7
7	5.63 ± 0.3	8.54 ± 0.5	3 ± 2.1

parameters and tilt angles for these 2D crystals with no interactions with the SAM. While the lattice parameters and tilt angles in the absence of the SAM are significantly different from those when the substrate is present, the odd–even effect on the tilt angles persists even without the presence of the SAM. Figure 4 compares the tilt angles of the two systems mentioned

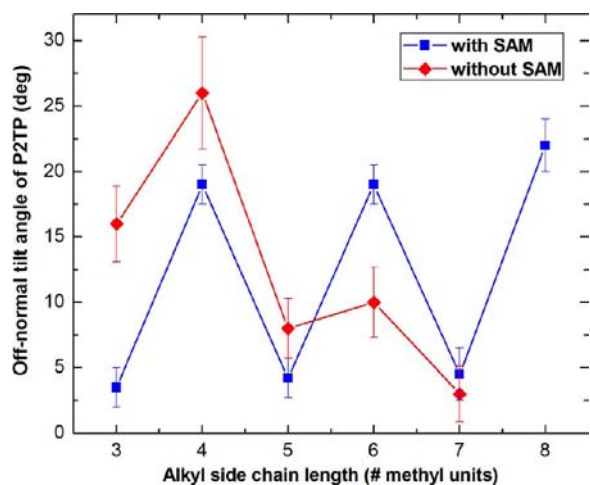


Figure 4. Comparison of P2TP off-normal tilt angles by simulation between the presence of an ODTS SAM (blue) and that with the absence of a SAM (red).

here, i.e., with and without a SAM present. Overall, the selection of a tilt angle preferred by each P2TP molecule is a cumulative effect of the interactions of the P2TP molecules among themselves, accentuated by interactions between the P2TP crystal and the SAM, and the topology of the surface (if a substrate is present). Thus, the odd–even effect is observed

whether the SAM is present or not (see the Supporting Information for more details). However, the odd–even effect is enhanced in the presence of an underlying SAM substrate.

The significant odd–even effect that we observed in the tilt angle of alkylated P2TP molecules on both HDTS and ODTS monolayers can potentially result in a similar odd–even effect in the strength of the electronic coupling between molecules along the plane of the substrate. This is the plane in which charge transport takes place in organic field-effect transistors (OFETs). To study the effect on the charge transport in OFETs, 40 nm thick films of C_N –P2TP– C_N were evaporated, after which the transistors were completed by evaporating 40 nm thick Au source-drain electrodes through a shadow mask. The AFM images showed two-dimensional grains with monolayer terraces (see Figure S5, Supporting Information). The OFETs were measured in an N_2 glovebox to exclude the effect of air on the devices. The electrical measurements and mobility calculations are provided in the Supporting Information. Figure 5 shows the saturated field-effect mobility

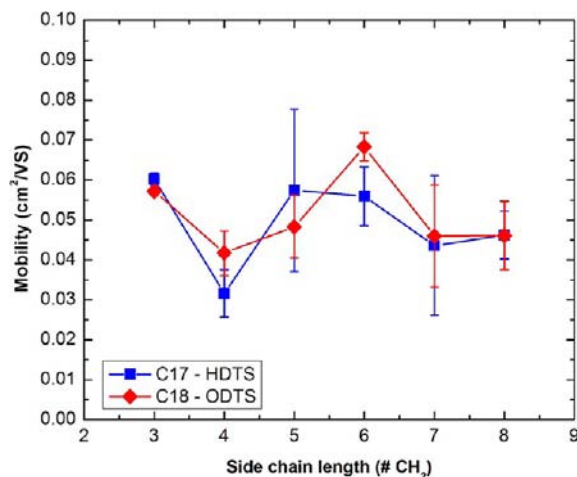


Figure 5. Field-effect mobility obtained on transistors with 40 nm thick films of C_N –P2TP– C_N . No clear trend with side chain length is observed within the error of measurement, which is likely due to other aspects that are the main limiting mechanism for charge transport: e.g., grain boundaries and/or the packing of the second and third molecular layer.

obtained from the transfer curves, where the source-drain current (I_{sd}) is plotted versus gate voltage (V_G). No clear dependence of the mobility was observed with increasing chain length and no differences in charge transport between OFETs using HDTS and ODTS treated substrates were observed; i.e., no odd–even effect was observed within the error of measurement.

The charges in the transistor channel are confined to the first few nanometers, and two to three layers of organic semiconductor dominate the charge transport.^{34,37} While the available X-ray data do not permit a structural refinement of a multilayer film comprised of very few layers, the similarity of the X-ray data between the submonolayer films and 2–3 layer thick films (not shown) strongly suggests that the odd–even effect persists for at least the first two to three layers. However, factors such as the density and type of grain boundaries are known to play a significant role in determining the overall device performance. Therefore, while an odd–even effect could still exist in the intrinsic charge carrier mobility, i.e., in

individual first monolayer grains of the different C_N -P2TP- C_N films, this effect is not necessarily reflected in the aggregate device performance. Nonetheless, we attempted to fabricate monolayer dimensional devices which would allow us to measure the transport solely in the first layer of the organic semiconductor. However, due to a strong dependence of the mobility on the second layer coverage,³⁴ the results showed a large variation and were inconclusive.

In order to estimate the impact of the odd–even effect on the intrinsic electronic coupling between the molecules in the C_N -P2TP- C_N layer, DFT calculations were performed for the packing obtained from the GIXD refinement. The transfer integrals for the HOMO orbitals were calculated^{55,56} for the neighboring dimers at the B3LYP/6-31G(d,p) level of theory^{57–61} as implemented in Q-Chem 3.2 quantum chemistry package.⁶² The solubilizing alkyl chains are known to have no significant effect on the transfer integrals and were therefore not included. The transfer integral values were computed for all four inequivalent next-nearest neighbor transitions (dimer pairs) in the unit cell, but only the three transitions indicated in Figure 2C (P, T1, T2) yielded nonzero transfer integral values. The results for these transitions are summarized in Table 5. An odd–even effect occurs in all three dimer

Table 5. Transfer Integral Values for Chain Lengths 3–7, Calculated at the B3LYP/6-31G(d,p) Level^a

N	dimer type		
	P (meV)	T1 (meV)	T2 (meV)
3	1.64	4.23	4.20
4	2.32	7.25	7.25
5	1.21	0.62	1.02
6	2.76	4.23	4.34
7	1.23	2.90	2.76

^a The dimer types (P, T1, T2) are indicated in the top-view unit cell in Figure 2C.

transitions, most pronounced in the diagonal transfer elements T1 and T2. Overall, these values suggest that there should indeed be an odd–even effect in the intrinsic hole conductivity (HOMO level). This effect was not observed experimentally due to the challenges discussed above.

CONCLUSIONS

The layered growth of C_N -P2TP- C_N , in which $N = 3–8$, was studied on crystalline monolayers of HDTS and ODTS. For the first monolayer of C_N -P2TP- C_N , an odd–even effect in tilt angle with increasing side chain length was observed by GIXD, with no observable differences between either HDTS- or ODTS-treated surfaces. The odd–even effect was theoretically verified by MD computations, where we observed that the tilting of the molecules oscillated between odd- and even-length alkyl chains even in the absence of a substrate. This can only mean that the phenomenon occurs as a result of the composite inter- and intramolecular interactions among molecules. The effect is increased by the presence of the SAM whose interactions of the P2TP molecules alter the lattice parameters and the magnitude of the tilting. We observed no tendency for molecules in this series to alter their crystal packing motif from the initial herringbone crystal structure; hence, this is not the origin of the odd–even effect. In the initial layer growth of C_N -P2TP- C_N on HDTS an additional phase of lying molecules was observed in AFM measurements, but not during the GIXD

investigations, suggesting that it might not be stable and could over time be converted to the respective standing (tilted or untilted) phases that is found on both HDTS and ODTS. Despite the pronounced odd–even effect in the film structure, no clear odd–even effect or dependence of side chain length on mobility was observed in FET measurements, which is likely due to the contribution of several layers to the charge transport and other limiting factors for charge transport, such as grain boundaries. In conclusion, we showed that small differences in dielectric surface or molecular structure can lead to significant effects during the growth of the first layers of organic compounds by thermal evaporation. The origins of these differences were further understood by MD simulations. Additional studies need to cover a different range of molecules with similar systematic variations to broaden the understanding between molecular structure and macroscale thin film morphology.

METHODS

Highly n-doped Si wafers with 300 nm thermally grown oxide were cleaned in a piranha solution (70:30 H_2SO_4/H_2O_2 ; caution highly reactive with organic compounds) and UV- O_3 treated for 5 min prior to spin coating. A solution of 3 mM hepta- or octadecyltrimethoxysilane in trichloroethylene was deposited on the Si/SiO₂ wafers and allowed to partially self-assemble for 10 s, after which the substrate was spun at 3000 rpm. The substrates were subsequently placed in a closed container together with a small vial with hydrochloric acid for a period of >5 h to promote the bonding to SiO₂ by the hydrolysis of the anchoring group. Afterward, the samples were rinsed with toluene and water. The thin films of alkyl substituted P2TPs were thermally evaporated in a vacuum chamber ($<5 \times 10^{-6}$ Torr) at elevated substrate temperatures at a rate of 0.3–0.5 Å/s. For the field-effect transistors Au source-drain electrodes were thermally evaporated through a shadow mask at room temperature. Electrical characterization was done using a Keithley 4200 semiconductor analyzer.

Grazing incidence X-ray diffraction of the C_N -P2TP- C_N films was performed at the Stanford Synchrotron Radiation Lightsource (SSRL) on beamline 11-3. The diffracted intensity was recorded on a 2-D image plate (MAR-345) with a pixel size of 150 μm (2300 \times 2300 pixels). The samples were ~ 10 mm long in the direction of the beam path, and the detector was located at a distance of 400 mm from the sample center (distance calibrated using a Lanthanum hexaboride standard). The incidence angle was chosen in the range of 0.10–0.12° to optimize the signal-to-background ratio. The beam size was 50 μm \times 150 μm (vertically by horizontally), which resulted in a beam exposure on the sample 150 μm wide over the entire length of the 10 mm long sample. The data were distortion-corrected (θ -dependent image distortion introduced by planar detector surface) before performing quantitative analysis on the images using the software WxDiff.²²

ASSOCIATED CONTENT

Supporting Information

Chemical structures, characterization of HDTS and ODTS self-assembled monolayers, influence of substrate temperature on apparent grain size of P2TPs, grazing incidence X-ray diffraction, computer simulations, and transfer characteristics FETs. This material is available free of charge via the Internet at <http://pubs.acs.org>.

AUTHOR INFORMATION

Corresponding Author

zbao@stanford.edu

Present Addresses

[†](S.H.) Samsung Cheil Industries, Chemicals R&D Center, Gochun-Dong, Uiwang-Si, Gyeonggi-Do, Korea.

[#](H.B.A.) Holst Centre, High Tech Campus 31, 5656AE, Eindhoven, The Netherlands.

Notes

The authors declare no competing financial interest.

ACKNOWLEDGMENTS

We thank R. Stoltenberg and M. LeMieux for assistance with AFM analysis. H.B.A. and A.P.Z. acknowledge The Netherlands Organisation for Scientific Research (NWO) for support. Portions of this research were carried out at the Stanford Synchrotron Radiation Lightsource, a Directorate of SLAC National Accelerator Laboratory and an Office of Science User Facility operated for the U.S. Department of Energy Office of Science by Stanford University. Z.B. acknowledges support provided by the National Science Foundation Solid State Chemistry (DMR 0705687-002) and Air Force Office of Scientific Research (FA 9550-12-1-0190). A.P.K. acknowledges support provided by Award No. KUS-C1-018-02, made by the King Abdullah University of Science and Technology (KAUST) to Cornell's KAUST-CU energy center. Intel Corp. and Harvard FAS Research Computing are thanked for the provision of computing resources. S.A. and A.A.G. thank the Stanford Global Climate and Energy Project and the National Science Foundation (DMR-0820484) and Department of Energy (DE-SC0008733) as well as the Corning Foundation for their generous support.

REFERENCES

- (1) Van den Brand, J.; de Baets, J.; van Mol, T.; Dietzel, A. *Microelectronics Reliability* **2008**, *48*, 1123–1128.
- (2) Su, S.-J.; Gonmori, E.; Sasabe, H.; Kido, J. *Adv. Mater.* **2008**, *22*, 5003–5007.
- (3) Piliago, C.; Holcombe, T. W.; Douglas, J. D.; Woo, C. H.; Beaujuge, P. M.; Fréchet, J. M. J. *J. Am. Chem. Soc.* **2010**, *132*, 7595–7597.
- (4) Chu, T.-Y.; Lu, J.; Beaupré, S.; Zhang, Y.; Pouliot, J.-R.; Wakim, S.; Zhou, J.; Leclerc, M.; Li, Z.; Ding, J.; Tao, Y. *J. Am. Chem. Soc.* **2011**, *133*, 4250–4253.
- (5) Gelinck, G. H.; Huitema, H. E. A.; van Veenendaal, E.; Cantatore, E.; Schrijnemakers, L.; van der Putten, J. B. P. H.; Geuns, T. C. T.; Beenhakkers, M.; Giesbers, J. B.; Huisman, B.-H.; Meijer, E. J.; Benito, E. M.; Touwslager, F. J.; Marsman, A. W.; van Rens, B. J. E.; de Leeuw, D. M. *Nat. Mater.* **2004**, *3*, 106–110.
- (6) Sekitani, T.; Nakajima, H.; Maeda, H.; Fukushima, T.; Aida, T.; Hata, K.; Someya, T. *Nat. Mater.* **2009**, *8*, 494–499.
- (7) Sele, C. W.; Kjellander, B. K. C.; Niesen, B.; Thornton, M. J.; van der Putten, J. B. P. H.; Myny, K.; Wöndergem, H. J.; Moser, A.; Resel, R.; van Breemen, A. J. J. M.; van Aerle, N.; Heremans, P.; Anthony, J. E.; Gelinck, G. H. *Adv. Mater.* **2009**, *21*, 4926–4931.
- (8) Yang, S. Y.; Shin, K.; Park, C. E. *Adv. Funct. Mater.* **2005**, *15*, 1806–1814.
- (9) Rivnay, J.; Jimison, L. H.; Northrup, J. E.; Toney, M. F.; Noriega, R.; Lu, S.; Marks, T. J.; Facchetti, A.; Salleo, A. *Nat. Mater.* **2009**, *8*, 952–958.
- (10) Bräuer, B.; Kukreja, R.; Virkar, A.; Akkerman, H. B.; Fognini, A.; Tyliczszak, T.; Bao, Z. *Org. Electron.* **2011**, *12*, 1936–1942.
- (11) Verploegen, E.; Mondal, R.; Bettinger, C. J.; Sok, S.; Toney, M. F.; Bao, Z. *Adv. Funct. Mater.* **2010**, *20*, 3519–3529.
- (12) Coropceanu, V.; Cornil, J.; da Silva Filho, D. A.; Olivier, Y.; Silbey, R.; Brédas, J.-L. *Chem. Rev.* **2007**, *107*, 926–952.
- (13) Brédas, J.-L.; Cornil, J.; Beljonne, D.; dos Santos, D. A.; Shuai, Z. *Acc. Chem. Res.* **1999**, *32*, 267–276.
- (14) Park, S. K.; Jackson, T. N.; Anthony, J. E.; Mourey, D. A. *Appl. Phys. Lett.* **2007**, *91*, 063514.
- (15) Reese, C.; Roberts, M. E.; Parkin, S. R.; Bao, Z. *Appl. Phys. Lett.* **2009**, *94*, 202101.
- (16) Okamoto, T.; Nakahara, K.; Saeki, A.; Seki, S.; Oh, J. H.; Akkerman, H. B.; Bao, Z.; Matsuo, Y. *Chem. Mater.* **2011**, *23*, 1646–1649.
- (17) Gsänger, M.; Oh, J. H.; Könemann, M.; Höffken, H. W.; Krause, A.-M.; Bao, Z.; Würthner, F. *Angew. Chem., Int. Ed.* **2010**, *49*, 740–743.
- (18) MacGillivray, L. R. *CrystEngComm* **2004**, *6*, 77.
- (19) Ward, M. D. *MRS Bull.* **2011**, *30*, 705–712.
- (20) Giri, G.; Verploegen, E.; Mannsfeld, S. C. B.; Atahan-Evrenk, S.; Kim, D. H.; Lee, S. Y.; Becerril, H. A.; Aspuru-Guzik, A.; Toney, M. F.; Bao, Z. *Nature* **2011**, *480*, 504–508.
- (21) Yang, J.; Yan, D. *Chem. Soc. Rev.* **2009**, *38*, 2634.
- (22) Mannsfeld, S. C. B.; Tang, M. L.; Bao, Z. *Adv. Mater.* **2011**, *23*, 127–131.
- (23) Mannsfeld, S. C. B.; Virkar, A.; Reese, C.; Toney, M. F.; Bao, Z. *Adv. Mater.* **2009**, *21*, 2294–2298.
- (24) Yuan, Q.; Mannsfeld, S. C. B.; Tang, M. L.; Roberts, M.; Toney, M. F.; DeLongchamp, D. M.; Bao, Z. *Chem. Mater.* **2008**, *20*, 2763–2772.
- (25) Garnier, F.; Yassar, A.; Hajlaoui, R.; Horowitz, G.; Deloffre, F.; Servet, B.; Ries, S.; Alnot, P. *J. Am. Chem. Soc.* **1993**, *115*, 8716–8721.
- (26) Meng, H.; Bao, Z.; Lovinger, A. J.; Wang, B.-C.; Mujsce, A. M. *J. Am. Chem. Soc.* **2001**, *123*, 9214–9215.
- (27) Yuan, Q.; Mannsfeld, S. C. B.; Tang, M. L.; Roberts, M.; Toney, M. F.; DeLongchamp, D. M.; Bao, Z. *Chem. Mater.* **2008**, *20*, 2763–2772.
- (28) Tang, M. L.; Reichardt, A. D.; Okamoto, T.; Miyaki, N.; Bao, Z. *Adv. Funct. Mater.* **2008**, *18*, 1579–1585.
- (29) Ebata, H.; Izawa, T.; Miyazaki, E.; Takimiya, K.; Ikeda, M.; Kuwabara, H.; Yui, T. *J. Am. Chem. Soc.* **2007**, *129*, 15732–15733.
- (30) Crone, B.; Dodabalapur, A.; Lin, Y.-Y.; Filas, R. W.; Bao, Z.; LaDuca, A.; Sarpeshkar, R.; Katz, H. E.; Li, W. *Nature* **2000**, *403*, 521–523.
- (31) Oh, J. H.; Liu, S.; Bao, Z.; Schmidt, R.; Würthner, F. *Appl. Phys. Lett.* **2007**, *91*, 212107.
- (32) Tao, F.; Bernasek, S. L. *Chem. Rev.* **2007**, *107*, 1408–1453.
- (33) Gupta, V.; Abbott, N. *Phys. Rev. E* **1996**, *54*, R4540–R4543.
- (34) Huang, J.; Sun, J.; Katz, H. E. *Adv. Mater.* **2008**, *20*, 2567–2572.
- (35) Sung, A.; Ling, M. M.; Tang, M. L.; Bao, Z.; Locklin, J. *Chem. Mater.* **2007**, *19*, 2342–2351.
- (36) Vaidyanathan, S.; Dötz, F.; Katz, H. E.; Lawrentz, U.; Granstrom, J.; Reichmanis, E. *Chem. Mater.* **2007**, *19*, 4676–4681.
- (37) Dinelli, F.; Murgia, M.; Levy, P.; Cavallini, M.; Biscarini, F.; de Leeuw, D. *Phys. Rev. Lett.* **2004**, *92*, 116802.
- (38) Kim, C. S.; Jo, S. J.; Lee, S. W.; Kim, W. J.; Baik, H. K.; Lee, S. J. *Adv. Funct. Mater.* **2007**, *17*, 958–962.
- (39) Xia, Y.; Cho, J. H.; Lee, J.; Ruden, P. P.; Frisbie, C. D. *Adv. Mater.* **2009**, *21*, 2174–2179.
- (40) Bürgi, L.; Richards, T. J.; Friend, R. H.; Siringhaus, H. *J. Appl. Phys.* **2003**, *94*, 6129.
- (41) Mathijssen, S. G. J.; Kemerink, M.; Sharma, A.; Cölle, M.; Bobbert, P. A.; Janssen, R. A. J.; de Leeuw, D. M. *Adv. Mater.* **2008**, *20*, 975–979.
- (42) Chua, L.-L.; Zaumseil, J.; Chang, J.-F.; Ou, E. C.-W.; Ho, P. K.-H.; Siringhaus, H.; Friend, R. H. *Nature* **2005**, *434*, 194–199.
- (43) Sharma, A.; Mathijssen, S.; Smits, E.; Kemerink, M.; de Leeuw, D.; Bobbert, P. *Phys. Rev. B* **2010**, *82*, 075322.
- (44) Sharma, A.; Mathijssen, S. G. J.; Cramer, T.; Kemerink, M.; de Leeuw, D. M.; Bobbert, P. A. *Appl. Phys. Lett.* **2010**, *96*, 103306.
- (45) Lim, S.; Kim, S.; Lee, J.; Kim, M.; Kim, D.; Zyung, T. *Synth. Met.* **2005**, *148*, 75–79.
- (46) Virkar, A.; Mannsfeld, S.; Oh, J. H.; Toney, M. F.; Tan, Y. H.; Liu, G.; Scott, J. C.; Miller, R.; Bao, Z. *Adv. Funct. Mater.* **2009**, *19*, 1962–1970.

- (47) Ito, Y.; Virkar, A. A.; Mannsfeld, S.; Oh, J. H.; Toney, M.; Locklin, J.; Bao, Z. *J. Am. Chem. Soc.* **2009**, *131*, 9396–9404.
- (48) Choudhary, D.; Clancy, P.; Bowler, D. R. *Surf. Sci.* **2005**, *578*, 20–26.
- (49) Verlaak, S.; Steudel, S.; Heremans, P.; Janssen, D.; Deleuze, M. *Phys. Rev. B* **2003**, *68*, 195409.
- (50) Virkar, A. A.; Mannsfeld, S. C. B.; Bao, Z. *J. Mater. Chem.* **2010**, *20*, 2664.
- (51) Locklin, J.; Roberts, M.; Mannsfeld, S.; Bao, Z. *Polymer Rev.* **2006**, *46*, 79–101.
- (52) Kaganer, V.; Möhwald, H.; Dutta, P. *Rev. Mod. Phys.* **1999**, *71*, 779–819.
- (53) Kaushik, A. P.; Clancy, P. *Surf. Sci.* **2011**, *605*, 1185–1196.
- (54) Haran, M.; Goose, J. E.; Clote, N. P.; Clancy, P. *Langmuir* **2007**, *23*, 4897–4909.
- (55) Norton, J. E.; Brédas, J.-L. *J. Chem. Phys.* **2008**, *128*, 034701.
- (56) Senthilkumar, K.; Grozema, F. C.; Bickelhaupt, F. M.; Siebbeles, L. D. A. *J. Chem. Phys.* **2003**, *119*, 9809.
- (57) Becke, A. D. *J. Chem. Phys.* **1993**, *98*, 5648.
- (58) Lee, C.; Yang, W.; Parr, R. G. *Phys. Rev. B* **1988**, *37*, 785–789.
- (59) Francl, M. M. *J. Chem. Phys.* **1982**, *77*, 3654.
- (60) Hariharan, P. C.; Pople, J. A. *Theor. Chim. Acta* **1973**, *28*, 213–222.
- (61) Hehre, W. J. *J. Chem. Phys.* **1972**, *56*, 2257.
- (62) Shao, Y.; Molnar, L. F.; Jung, Y.; Kussmann, J.; Ochsenfeld, C.; Brown, S. T.; Gilbert, A. T. B.; Slipchenko, L. V.; Levchenko, S. V.; O'Neill, D. P.; DiStasio, R. A., Jr.; Lochan, R. C.; Wang, T.; Beran, G. J. O.; Besley, N. A.; Herbert, J. M.; Yeh Lin, C.; Van Voorhis, T.; Hung Chien, S.; Sodt, A.; Steele, R. P.; Rassolov, V. A.; Maslen, P. E.; Korambath, P. P.; Adamson, R. D.; Austin, B.; Baker, J.; Byrd, E. F. C.; Dachselt, H.; Doerksen, R. J.; Dreuw, A.; Dunietz, B. D.; Dutoi, A. D.; Furlani, T. R.; Gwaltney, S. R.; Heyden, A.; Hirata, S.; Hsu, C.-P.; Kedziora, G.; Khalliulin, R. Z.; Klunzinger, P.; Lee, A. M.; Lee, M. S.; Liang, W.; Lotan, I.; Nair, N.; Peters, B.; Proynov, E. I.; Pieniazek, P. A.; Min Rhee, Y.; Ritchie, J.; Rosta, E.; David Sherrill, C.; Simmonett, A. C.; Subotnik, J. E.; Lee Woodcock, H., III; Zhang, W.; Bell, A. T.; Chakraborty, A. K.; Chipman, D. M.; Keil, F. J.; Warshel, A.; Hehre, W. J.; Schaefer, H. F., III; Kong, J.; Krylov, A. I.; Gill, P. M. W.; Head-Gordon, M. *Phys. Chem. Chem. Phys.* **2006**, *8*, 3172.